Fuel Processing Technology 211 (2021) 106593

Contents lists available at ScienceDirect

Fuel Processing Technology

journal homepage: www.elsevier.com/locate/fuproc

Research article

Comparison study of fusibility between coal ash and synthetic ash

Zong-shuai Yuan[a,b], Ji Wang[a,b], Lingxue Kong[a], Jin Bai[a,*], Zhonghai Ni[c], Huaizhu Li[a], Zongqing Bai[a], Wen Li[a]

[a] State Key Laboratory of Coal Conversion, Institute of Coal Chemistry, Chinese Academy of Sciences, Taiyuan 030001, PR China
[b] University of Chinese Academy of Sciences, Beijing 100049, PR China
[c] School of Chemical Engineering and Technology, China University of Mining and Technology, Xuzhou 221116, PR China

ARTICLE INFO

Keywords:
Fusibility
Coal ash
Synthetic ash
Comparison

ABSTRACT

Coal ash fusibility plays an essential role in selecting coal and determining operation condition for different gasifiers. To understand main factors on ash fusibility for adjustment, the synthetic ash which composed of pure oxides is widely used in previous study instead of the real coal ash. However, the comparison on fusibility between coal ash (CA) and synthetic ash (SA) is still unknown. In this study, four typical coals were selected to compare fusibility between CA and SA. The results indicated that the SA is not suitable to simulate all CA for fusibility study. For the ash with high-calcium-low-iron, SA can be used because of the same mineral transformation at high temperatures. The AFTs of the ash with high-calcium-high(medium)-iron is higher than that of SA, resulting from difference between gehlenite and akermanite. Mullite is detected in CA with low-calcium-low-iron, so the SA cannot replace CA to investigate fusibility for absence of mullite. Besides, fusibility of samples with low liquid content and high viscosity of liquid cannot be simulated by synthetic ash due to different mass transfer rate. The ashes with chemical compositions located in high-melting-temperature region shows an obvious different fusibility between CA and SA because of the low liquid content.

1. Introduction

Gasification is widely recognized as an important method to achieve the efficient and clean utilization of coal for China [1–4]. In the gasifiers, organic matters transforms into syngas while mineral matters converts into ash or slag at high temperature [5]. The molten ash tends to cause ash-related problems, such as deposition, fouling and slagging, which significantly influences operation of the gasifier [6–8]. Compared to viscosity and rheological property of coal ash, ash fusibility is the most basic and important parameter to investigate ash-related problems [9]. Therefore, many investigations have studied ash fusibility in coal gasification.

Ash fusibility is commonly characterized by ash fusion temperatures (AFTs) which determined by specific physical geometry of ash cone during heating, including deformation temperature (DT), softening temperature (ST), hemisphere temperature (HT) and flow temperature (FT) [10]. Ash fusion is a process of which coal ash gradually converts from solid phase to liquid phase during heating which is mainly dependent on minerals [5,11]. In addition, the content and viscosity of liquid phase also affect ash fusion behavior via mass transfer [12–15].

Fusibility is essentially affected by the chemical and mineral composition of coal ash, as well as the interaction between them [5,16]. According to influence on ash fusion temperatures, minerals in coal ash are usually classified as refractory minerals and fluxing minerals. The refractory minerals mainly include mullite (melting point: 1810 °C), quartz (melting point: 1610 °C), and rutile (melting point: 1720 °C), and the fluxing minerals are usually anhydrite (melting point: 1200 °C), albite (melting point: 1100 °C), calcium silicate (melting point: 1540 °C) and anorthite (melting point: 1553 °C) [17,18]. Due to complexity of minerals in coal ash, chemical composition of coal ash is usually measured and expressed in form of oxides, such as SiO_2, Al_2O_3, CaO, MgO, Fe_2O_3, TiO_2, K_2O, Na_2O, SO_3, P_2O_5 [19,20]. Those oxides can be divided into acidic oxide (SiO_2, Al_2O_3 and TiO_2) and basic oxide (CaO, MgO, Fe_2O_3, K_2O, Na_2O, SO_3) based on their roles on fusibility in terms of ionic potential (valence divided by ionic radius) [21].

In recent years, the influence of chemical composition on the ash fusibility has been investigated by many researchers [14,22–25]. As four constituents (SiO_2, Al_2O_3, Fe_2O_3 and CaO) usually account for more than 80% of coal ash, some researchers considered that influence of K_2O, Na_2O, TiO_2, MgO and SO_3 on ash fusibility can be ignored due to their low concentrations [9,12,23]. To simplify research system of coal ash, SiO_2-Al_2O_3-CaO-Fe_2O_3 quaternary system of synthetic ash has

* Corresponding author.
E-mail address: stone@sxicc.ac.cn (J. Bai).

https://doi.org/10.1016/j.fuproc.2020.106593
Received 20 May 2020; Received in revised form 22 July 2020; Accepted 4 September 2020
0378-3820/ © 2020 Elsevier B.V. All rights reserved.

been widely used to simulate coal ash to study the ash fusibility [26–28]. Yan et al. [12] selected the synthetic ash to study ash fusion behavior by TMA (thermal mechanical analysis), and founded that ash fusion process consisted of three different stages, which was largely influenced by SiO_2/Al_2O_3. He et al. [29] established predictive models for iron transformation based on chemical composition, temperature and atmosphere as well as slag residence by using synthetic ash. And the model was suitable to predict iron distribution of Yanzhou ash in Shell gasifier. Song et al. [30] and Liu et al. [23] both studied the effect of SiO_2/Al_2O_3 on AFTs, but opposite results were acquired because one sample was real coal ash and the other one was synthetic ash. Although the chemical composition is similar between real coal ash and synthetic ash, mineral matters differs from each other in many ways. Consequently, mineral reactions of real coal ash and synthetic ash maybe different, which will result in different fusibility. It is still a problem that what kind of synthetic ash can be used to study fusibility of the real coal ash. However, little research has reported on difference of fusibility between the real coal ash and the synthetic ash. Hence, it is necessary to verify the synthetic ash method in ash fusibility study.

In this work, we selected four real coal ashes with different chemical compositions, and prepared their synthetic ashes in SiO_2-Al_2O_3-CaO-MgO-Fe_2O_3-TiO_2-K_2O-Na_2O-SO_3 system. The AFTs of the real coal ashes and the synthetic ashes were measured to compare their ash fusibility. X-ray diffraction (XRD) and FactSage were used to characterize mineral transformation of the real coal ashes and the synthetic ashes.

2. Experimental

2.1. Samples

Four typical real coal ashes were selected in this study, and prepared following the Chinese standard GB/T1574–2007. The chemical composition of coal ashes was analyzed by XRF (X-ray fluorescence) according to ASTM D6349, and the results are presented in Table 1. The four coal ashes can be characterized by high-calcium-low-iron (CaO = 14.33%, Fe_2O_3 = 6.43%) (designated as CA-1), high-calcium-medium-iron (CaO = 37.60%, Fe_2O_3 = 9.80%) (designated as CA-2), high-calcium-high-iron (CaO = 25.17%, Fe_2O_3 = 19.14%) (designated as CA-3) and low-calcium-low-iron (CaO = 3.84%, Fe_2O_3 = 4.47%) (designated as CA-4), respectively [31]. The A/B (acid/base = (SiO_2 + Al_2O_3 + TiO_2)/(Fe_2O_3 + CaO + MgO + Na_2O + K_2O + SO_3)) [21,32] and Si/Al (SiO_2/Al_2O_3 weight ratio) are also given in Table 2.

According to chemical composition of the real coal ashes, synthetic ashes (designated as SA-1, SA-2, SA-3, and SA-4, respectively) were prepared with chemical reagents (SiO_2, Al_2O_3, Fe_2O_3, CaO, MgO, $CaSO_4$, TiO_2, K_2CO_3 and Na_2CO_3). P_2O_5 was not considered in the synthetic ash as its concentration is lower than 0.5%. Na_2O and K_2O were added in form of Na_2CO_3 and K_2CO_3, respectively [9,33,34]. Besides, $CaSO_4$ was selected to stimulate SO_3 in the synthetic ash [35], and addition of CaO in synthetic ash is equal to the content of CaO in coal ash minus the content of CaO in $CaSO_4$. Those chemical reagents were ground to particle diameter less than 75 μm and calcined at 815 °C for 1 h to be dehydrated fully separately, and then blended in an agate mortar. Besides, in order to confirm whether the mineral phase of synthetic ash changes when the temperature increases to 815 °C, the synthetic ashes were also calcined according to GB/T1574–2007 and designated as SA815.

Table 2
A/B and Si/Al of the real coal ashes.

Sample	CA-1	CA-2	CA-3	CA-4
Si/Al	2.17	2.61	2.40	2.41
A/B	2.32	0.61	0.61	5.94

2.2. Ash fusion temperatures test

AFTs of CA, SA and SA815 were test by 5E-AF4115 with a maximum test temperature of 1550 °C according to the Chinese standard procedure GB/T 219-2008 under reducing (CO/CO_2 volume ratio = 6:4) atmosphere [10]. Four characteristic temperatures, namely deformation temperature (DT), softening temperature (ST), hemisphere temperature (HT) and flow temperature (FT) were automatically recorded by detecting system in terms of the geometrical changes of ash cone during heating. The heating rate was 15 °C/min from ambient temperature to 900 °C, and then 5 °C/min to 1550 °C.

2.3. Preparation and characterization of quenched slag

To explore the effect of mineral transformation on AFTs of CA and SA, the ash sample (1.0 g) was placed in a corundum crucible, and heated in horizontal furnace under reducing (CO/CO_2 volume ratio = 6:4) atmosphere. The sample was preheated in low temperature zone (about 900 °C) for 15 s, and then moved to target temperature zone for 15 min. Finally, the sample was pulled out and quenched into ice-water. The target temperature was chosen by AFTs of ash sample (around from DT to FT with an interval of 50 °C).

The quenched slag was ground to particle less than 75 μm in diameter. Minerals of the ash samples was recorded by PANalytical X'Pert3 powder diffractometer at a voltage of 40 kV and a current of 40 mA with Cu Kα radiation (1.541874 A), and the focusing (Bragg-Brentano) optics was used. The samples were scanned with a step interval of 0.02° at 4°/min over a 2θ of 5–80°. Mineral phase of quenched slag was analyzed by the software package EVA.

2.4. FactSage calculations

Thermodynamic software package FactSage based on minimization of Gibbs energy was applied to calculate multiphase equilibria, content of solid liquid phases from ash composition [36–38]. It is worth noting that mass transfer, heat transfer and kinetic limitation are not considered in FactSage [14,39]. In this work, FactSage 7.3 with FToxid and FactPS was used to calculate mineral compositions and viscosity. Eight components including SiO_2, Al_2O_3, Fe_2O_3, CaO, MgO, TiO_2, Na_2O and K_2O were input into calculation, because the existence state of SO_3 is gas phase above 1000 °C [14]. Calculations were carried out from 800 to 1600 °C with an interval of 50 °C under the reducing atmosphere (60% CO and 40% CO_2, volume ratio). Equilib, phase Diagram and viscosity were used to calculate phase transformation, ternary phase diagram and viscosity of liquid phase, respectively.

Table 1
Chemical composition of the real coal ashes (wt%).

Sample	SiO_2	Al_2O_3	Fe_2O_3	CaO	MgO	SO_3	TiO_2	K_2O	Na_2O	P_2O_5	Others
CA-1	46.16	21.30	6.43	14.33	0.94	5.14	0.80	1.29	1.34	0.17	2.10
CA-2	26.28	10.06	9.80	37.60	1.24	8.59	0.52	0.37	2.68	0.02	2.84
CA-3	25.79	10.75	19.14	25.17	3.34	10.58	0.43	0.56	1.41	0.04	2.79
CA-4	58.76	24.40	4.47	3.84	1.45	1.91	1.02	1.78	0.72	0.49	1.16

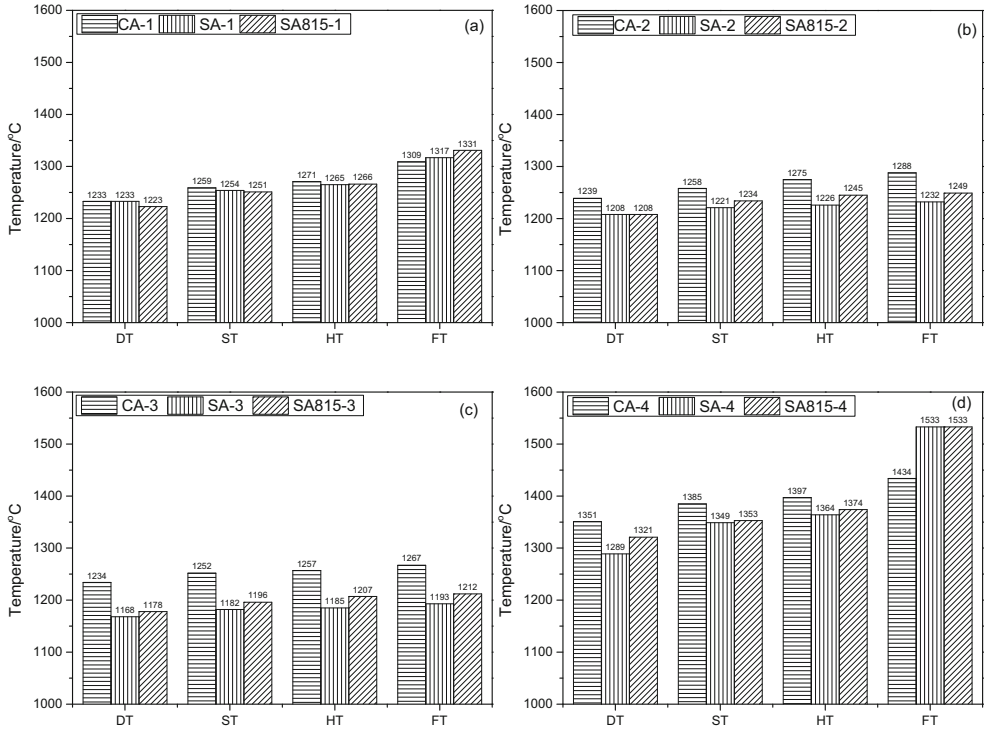


Fig. 1. Ash fusion temperatures of the ashes.

3. Results and discussion

3.1. AFTs of CA, SA and SA815

As shown in Fig. 1, AFTs of CA-1 is similar with that of CA-2 and CA-3, while they are lower than that of CA-4. This is attributed to Si/Al and base-to-acid (A/B) ratio (Table 2) [21,30]. Pervious work showed that the fusibility of coal ash increases with the increase of A/B. The four ash samples have similar Si/Al (about 2.40), while the A/B of CA-4 (5.94) is higher than that of other three ashes. This explains why AFTs of CA-4 is higher than that of other three ashes. Besides, the AFTs of SA are similar with that of CA, which demonstrates that it is reasonable to compare difference on AFTs of coal ash by using synthetic ash.

Fig. 1 also presents the difference of AFTs between CA, SA and SA815. The difference of AFTs between CA-1 and SA-1 is less than 10 °C. However, the AFTs of CA-2 and CA-3 are slightly higher than that of their synthetic ash (< 75 °C). Although DT, ST and HT of CA-4 are slightly higher than those of SA-4 (< 75 °C), the FT of CA-4 is 99 °C lower than that of SA-4. In addition, it was found that all AFTs difference between SA and SA815 is within 20 °C, indicating that property of the synthetic ash was not affected after 815 °C calcined. Therefore, discussion about AFTs of SA815 was not considered in the following.

3.2. Mineral transformation of CA and SA

The AFTs of a coal is largely dependent on its mineral matter compositions and variations therein as the temperature is increased. To explain different fusibility between the coal ash and the synthetic ash, mineral transformation experiment was carried out at high temperature.

As shown in Fig. 2(a), major minerals in CA-1 are quartz (SiO_2), lime (CaO), hematite (Fe_2O_3) and anhydrite ($CaSO_4$) at 815 °C. At 1200 °C, albite ($NaAlSi_3O_8$) and potassium feldspar ($KAlSi_3O_8$) form in ash, while the content of quartz decreases. As temperature increases, contents of albite and potassium feldspar continuously decrease and they disappear at 1400 °C. Hence, reactions among minerals at high temperature are summarized below:

$$Na_2O + SiO_2 + Al_2O_3 \rightarrow NaAlSi_3O_8 \text{ (albite)} \quad (1)$$

$$K_2O + SiO_2 + Al_2O_3 \rightarrow KAlSi_3O_8 \text{ (potassium feldspar)} \quad (2)$$

As for SA-1, quartz (SiO_2), lime (CaO), hematite (Fe_2O_3), anhydrite ($CaSO_4$) and corundum (Al_2O_3) are major minerals at 815 °C (Fig. 2(b)), which indicates that reaction does not occur between chemical reagents. Albite ($NaAlSi_3O_8$), potassium feldspar ($KAlSi_3O_8$) and anorthite ($CaAl_2Si_2O_8$) were found at 1200 °C. When temperature increases from 1250 °C to 1400 °C, the content of albite decreases and potassium feldspar reacts with anorthite to form low temperature eutectics, forming amorphous matter. The reactions in SA-1 are summarized below:

$$Na_2O + SiO_2 + Al_2O_3 \rightarrow NaAlSi_3O_8 \text{ (albite)} \quad (3)$$

$$K_2O + SiO_2 + Al_2O_3 \rightarrow KAlSi_3O_8 \text{ (potassium feldspar)} \quad (4)$$

$$CaSO_4 \rightarrow CaO + SO_3 \quad (5)$$

$$CaO + SiO_2 + Al_2O_3 \rightarrow CaAl_2Si_2O_8 \text{ (anorthite)} \quad (6)$$

The intensity of quartz in SA is higher than that in CA at 815 °C. Compared with SA, SiO_2 in CA exists in form of quartz and other minerals such as albite and potassium feldspar. At high temperatures, major minerals in both CA-1 and SA-1 are feldspar, which accounts for small difference of their AFTs. Furthermore, the low AFTs of SA-1 is attributed to formation of albite (melting point: 1100 °C) and low temperature eutectics between potassium feldspar (melting point: 1290 °C) and anorthite (melting point: 1553 °C).

In Fig. 3(a), quartz (SiO_2), lime (CaO), hematite (Fe_2O_3) and anhydrite ($CaSO_4$) are identified at 815 °C. Gehlenite ($Ca_2Al_2SiO_7$) and calcium silicate (Ca_2SiO_4) are detected at 1150 °C while peak intensity of quartz and anhydrite decreases [14]. This illustrates that quartz react with anhydrite to form gehlenite and calcium silicate. As temperature increases, contents of gehlenite and calcium silicate remain constant. At 1350 °C, a great deal of non-crystalline forms due to the formation of low temperature eutectics which consists of gehlenite and calcium silicate. Therefore, the major mineral reactions in CA-2 can be summarized as follows:

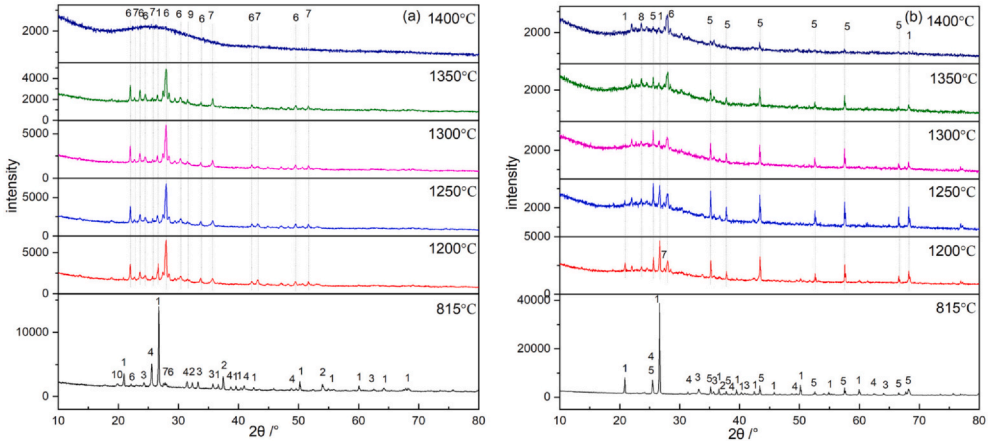


Fig. 2. XRD patterns of CA-1 (a) and SA-1(b) at different temperature.
1: quartz (SiO_2); 2: lime (CaO); 3: hematite (Fe_2O_3); 4: anhydrite ($CaSO_4$); 5: corundum (Al_2O_3); 6: albite ($NaAlSi_3O_8$); 7: potassium feldspar ($KAlSi_3O_8$); 8: anorthite ($CaAl_2Si_2O_8$); 9: gehlenite ($Ca_2Al_2SiO_7$); 10: kyanite (Al_2SiO_5).

$$CaSO_4 \rightarrow CaO + SO_3 \quad (7)$$

$$SiO_2 + Al_2O_3 + 2CaO \rightarrow Ca_2Al_2SiO_7\ (\text{gehlenite}) \quad (8)$$

$$2CaO + SiO_2 \rightarrow Ca_2SiO_4\ (\text{calcium silicate}) \quad (9)$$

Quartz (SiO_2), lime (CaO), hematite (Fe_2O_3), anhydrite ($CaSO_4$) and corundum (Al_2O_3) are main minerals in SA-2 at 815 °C (Fig. 3(b)), which is similar with that of CA-2 at 815 °C. At 1150 °C, the major minerals become akermanite ($Ca_2MgSi_2O_7$) and calcium silicate (Ca_2SiO_4) with a decrease of quartz and anhydrite. Akermanite ($Ca_2MgSi_2O_7$) reacts with calcium silicate at 1350 °C to form low temperature eutectics which is amorphous. Thus, reactions between minerals in SA-2 should be:

$$CaSO_4 \rightarrow CaO + SO_3 \quad (10)$$

$$2SiO_2 + MgO + 2CaO \rightarrow Ca_2MgSi_2O_7\ (\text{akermanite}) \quad (11)$$

$$2CaO + SiO_2 \rightarrow Ca_2SiO_4\ (\text{calcium silicate}) \quad (12)$$

It can be seen that the mineral matters of CA-2 differ from that of SA-2. Al_2O_3 exists in form of aluminosilicate in CA-2 while it is corundum in SA-2. Reactivity of the former is higher than that of the latter. As a result, quartz can react with Al_2O_3 in form of aluminosilicate and lime to form gehlenite (Eq. (8)) in CA-2. Table 3 lists Gibbs free energy of reactions among minerals calculated by FactSage. Because reactions with a low ΔG occurred easily, quartz preferred to react with MgO and lime to produce akermanite (Eq. (11)) in SA-2 at high temperature. As gehlenite (melting point: 1590 °C) is slightly hard to melt than akermanite (melting point: 1450 °C), the AFTs of CA-2 are higher (30–60 °C) than that of SA-2.

As shown in Fig. 4(a), major minerals in CA-3 are quartz (SiO_2), lime (CaO), hematite (Fe_2O_3) and anhydrite ($CaSO_4$) at 815 °C. Presence of gehlenite ($Ca_2Al_2SiO_7$) and spinel ($MgAl_2O_4$) suggests that quartz reacts with lime and corundum to generate gehlenite at 1150 °C as well as magnesia reacts with corundum to form spinel. Content of gehlenite decreases with increasing temperature and massive amorphous phase is detected at 1350 °C because of formation of low temperature eutectics. Reactions among minerals at high temperature in CA-3 are summarized below:

$$CaSO_4 \rightarrow CaO + SO_3 \quad (13)$$

$$SiO_2 + Al_2O_3 + 2CaO \rightarrow Ca_2Al_2SiO_7\ (\text{gehlenite}) \quad (14)$$

$$MgO + Al_2O_3 \rightarrow MgAl_2O_4\ (\text{spinel}) \quad (15)$$

As for SA-3, at 815 °C major minerals are quartz (SiO_2), hematite (Fe_2O_3), anhydrite ($CaSO_4$) and corundum (Al_2O_3) (Fig. 4(b)). At 1150 °C and 1200 °C, main minerals are akermanite ($Ca_2MgSi_2O_7$) and spinel ($MgAl_2O_4$). However, there is plenty of amorphous matter without crystal minerals at 1250 °C, ascribing to low temperature co-fusion of akermanite and spinel, which causes the decrease of AFTs of SA-3. Reactions among minerals at high temperature are summarized below:

$$CaSO_4 \rightarrow CaO + SO_3 \quad (16)$$

$$2SiO_2 + MgO + 2CaO \rightarrow Ca_2MgSi_2O_7\ (\text{akermanite}) \quad (17)$$

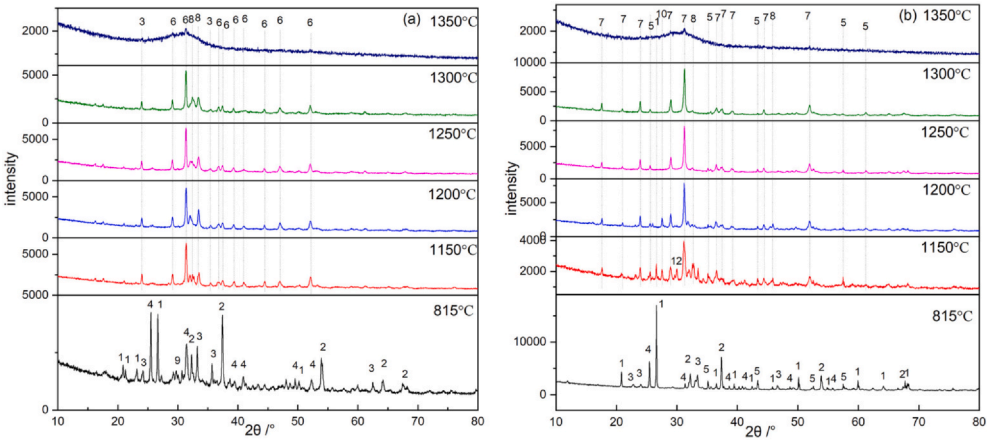


Fig. 3. XRD patterns of CA-2 (a) and SA-2 (b) at different temperature.
1: quartz (SiO_2); 2: lime (CaO); 3: hematite (Fe_2O_3); 4: anhydrite ($CaSO_4$); 5: corundum (Al_2O_3); 6: gehlenite ($Ca_2Al_2SiO_7$); 7: akermanite ($Ca_2MgSi_2O_7$); 8: calcium silicate (Ca_2SiO_4); 9: arcanite (K_2SO_4); 10: anatase (TiO_2); 11: nepheline ($NaAlSiO_4$); 12: wollastonite ($CaSiO_3$).

Table 3
Gibbs free energy of reactions among minerals at high temperature.

Reaction	ΔG/kJ·mol^{-1}			
	1150 °C	1200 °C	1250 °C	1300 °C
$SiO_2 + Al_2O_3 + 2CaO \rightarrow Ca_2Al_2SiO_7$ (gehlenite)	−167.94	−169.36	−170.79	−172.23
$2SiO_2 + MgO + 2CaO \rightarrow Ca_2MgSi_2O_7$ (akermanite)	−202.48	−203.09	−203.70	−204.31

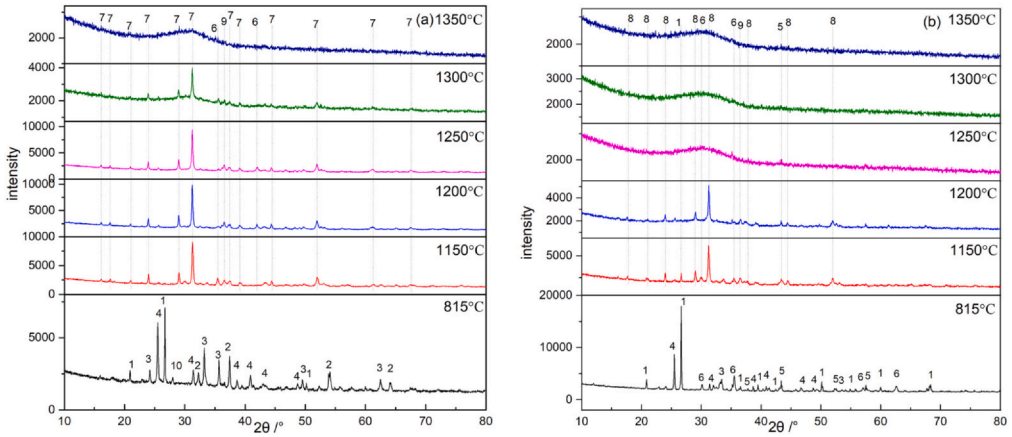


Fig. 4. XRD patterns of CA-3 (a) and SA-3 (b) at different temperature.
1: quartz (SiO_2); 2: lime (CaO); 3: hematite (Fe_2O_3); 4: anhydrite ($CaSO_4$); 5: corundum (Al_2O_3), 6: magnetite (Fe_3O_4); 7: gehlenite ($Ca_2Al_2SiO_7$); 8: akermanite ($Ca_2MgSi_2O_7$); 9: spinel ($MgAl_2O_4$); 10: kyanite (Al_2SiO_5).

$$MgO + Al_2O_3 \rightarrow MgAl_2O_4 \text{ (spinel)} \quad (18)$$

The mineral transformation between CA-3 and SA-3 is similar to that between CA-2 and SA-2. Therefore, the high AFTs of CA-3 is attributed to formation of gehlenite, and the low AFTs of SA-3 is due to formation of akermanite.

In Fig. 5(a), major minerals in CA-4 are quartz (SiO_2), anhydrite ($CaSO_4$), hematite (Fe_2O_3) with small amounts of muscovite ($KAl_2(Si_3O_{10})(OH)_2$) at 815 °C. At 1250 °C, Quartz reacts with Al_2O_3 in form of aluminosilicate to generate mullite ($2Al_2O_3{\cdot}SiO_2$) and kaolinite ($Al_2Si_2O_5(OH)_4$) decomposed into mullite. The content of mullite reduces with rising temperature until mullite disappears at 1500 °C and huge amount of amorphous matter occurs. Hence, reactions between minerals in CA-4 should be:

$$Al_2Si_2O_5(OH)_4 \text{ (Kaolinite)} \rightarrow Al_2O_3\ (\gamma) + 2Al_2O_3{\cdot}SiO_2 \text{ (mullite)} \quad (19)$$

$$SiO_2 + Al_2O_3 \rightarrow 2Al_2O_3{\cdot}SiO_2 \text{ (mullite)} \quad (20)$$

At 815 °C, quartz (SiO_2), anhydrite ($CaSO_4$), hematite (Fe_2O_3) as well as corundum (Al_2O_3) are major minerals in SA-4 (Fig. 5(b)). When temperature increases from 1250 °C to 1500 °C, formation of amorphous phase is attributed to the generation of low-temperature eutectics among the different oxides.

Due to formation of mullite (melting point: 1810 °C) in CA-4 below 1400 °C, DT, ST and HT of CA-4 are higher than that of SA-4. However, quartz (melting point: 1610 °C) and corundum (melting point: 2050 °C) in SA-4 above 1400 °C lead to the high FT of SA-4.

3.3. Thermal calculation of coal ash

Fig. 6 shows mineral compositions of the four ashes at high temperature under reducing atmosphere (CO/CO_2 volume ratio = 6:4), based on SiO_2-Al_2O_3-Fe_2O_3-CaO-MgO-TiO_2-K_2O-Na_2O calculated by FactSage. In Fig. 6(a), feldspar forms at high temperature in CA-1 leading to decrease of AFTs. Melilite and calcium silicate are dominant

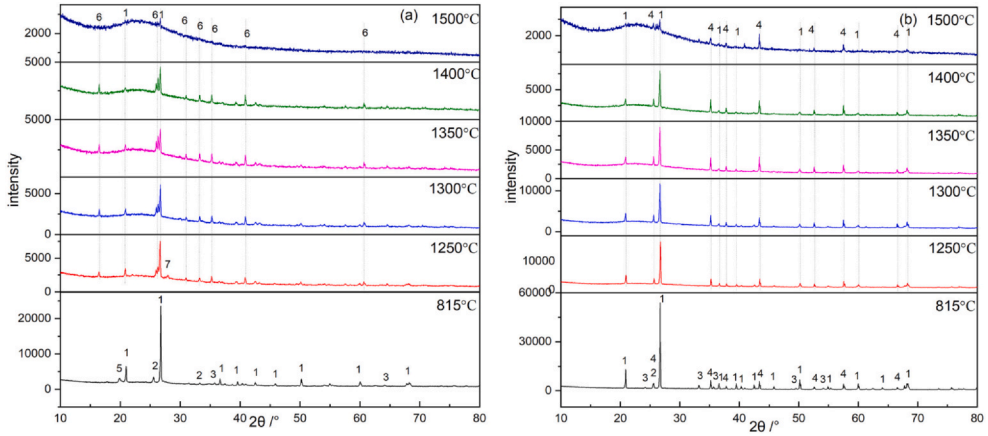


Fig. 5. XRD patterns of CA-4 (a) and SA-4 (b) at different temperature.
1: quartz (SiO_2); 2: anhydrite ($CaSO_4$); 3: hematite (Fe_2O_3); 4: corundum (Al_2O_3); 5: muscovite ($KAl_2(Si_3O_{10})(OH)_2$); 6: mullite ($2Al_2O_3{\cdot}SiO_2$); 7: albite ($NaAlSi_3O_8$).

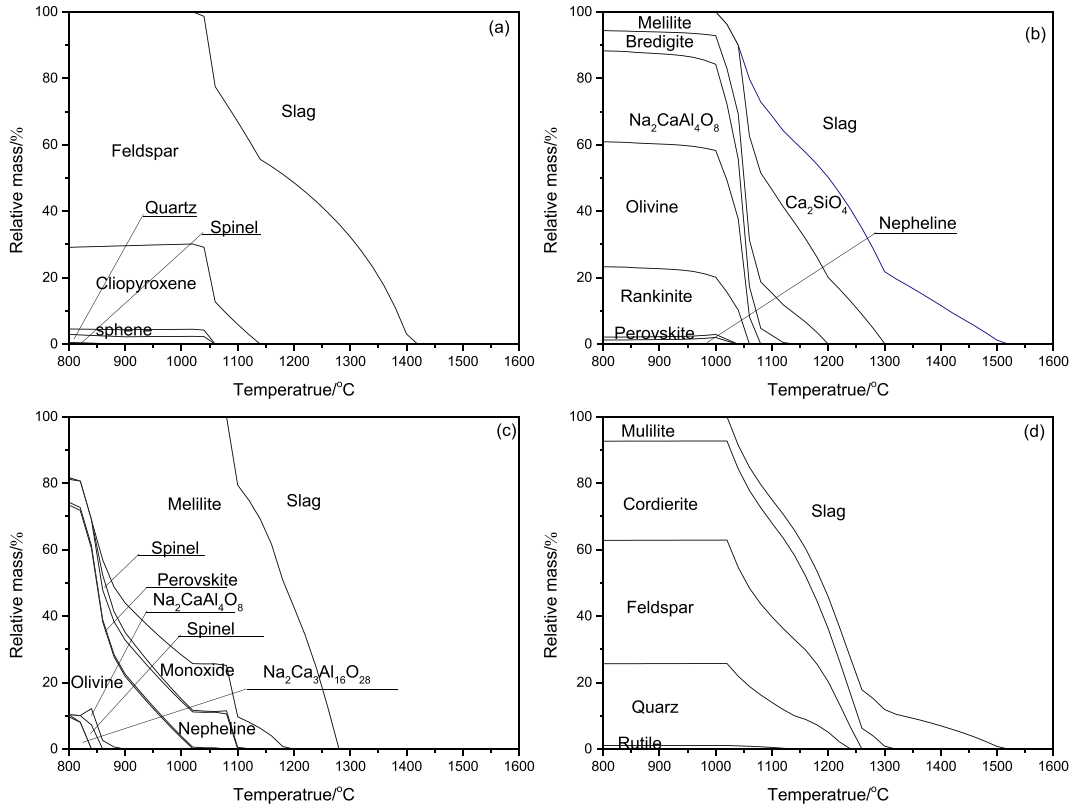


Fig. 6. FactSage calculation of the four ashes.
(a): ash-1; (b): ash-2; (c): ash-3; (d): ash-4.

minerals in CA-2 during 1150 °C to 1350 °C, which are same with the result of XRD in Fig. 3. In case of CA-3, melilite occurs at high temperature, which lowers AFTs of CA-2 and CA-3. Main mineral in CA-4 is mullite above 1250 °C, which is consistent with Fig. 5(a). It can be concluded that calculation results are well corresponded to experimental results of CA [18]. Due to complexity of minerals existed in CA, SA were prepared with chemical reagents, while mass transfer, heat transfer and kinetic limitation are not considered in reactions between the chemical oxides calculated by FactSage. Therefore, the calculation results are inconsistent with experimental results of SA.

Mineral matters of CA differ from that of SA. According to Fig. 6, SiO_2 exists in form of quartz, feldspar and clinopyroxene in CA-1 while only quartz in SA-1 (Fig. 2(b)), accounting for that diffraction intensity of SA-1 is stronger than CA-1. The presence of corundum in CA-2 are nepheline, melilite and $Na_2CaAl_4O_8$ which more easily react with quartz than corundum identified in SA-2. There is evident difference of minerals between CA-4 and SA-4. Compared to reaction of Table 3, it is difficult for quartz to react with corundum to form mullite in SA-4 according to Gibbs free energy of reaction (1300 °C, $\Delta G = -23.33$ kJ/mol) [18].

Ash fusion is a process that coal ash gradually converts from solid phase to liquid phase [14]. Mineral species is the dominant factor which affects mineral transformation behavior, while liquid viscosity and content also play an important role in formation of the initial liquid phase and melting of the residual solid phase [12,14]. Essentially, the viscosity and content of the liquid phase are also dependent on minerals and phases in ash. Their fusion processes of CA and SA are consistent in terms of thermodynamics. However, the mineral matters of CA and SA are different. For kinetics, if the viscosity of liquid phase is high or the content of liquid phase is low, the mineral transformation could be dominated by mass transfer. As a result, the difference of fusibility between CA and SA would be enlarged. The viscosity and content of liquid phase of coal ash at DT are shown in Fig. 7. During ash fusion

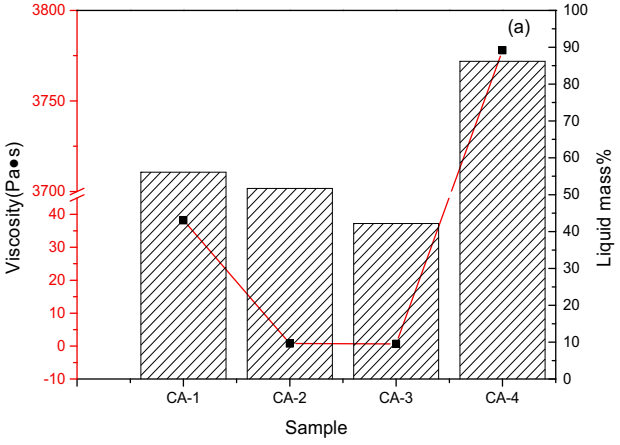


Fig. 7. The viscosity and content of liquid phase of ashes at DT.

process, the liquid viscosity was calculated according to composition of slag at DT. Small difference of fusibility between CA-1 and SA-1 is due to low viscosity (38 Pa·s) and high liquid content (56%). The viscosity of liquid phase of CA-2 and CA-3 is lower than 1 Pa·s and the liquid content is from 40% to 50%. Therefore, in terms of mass transfer, there is no obvious effect on the different fusibility between the CA and SA. However, the viscosity of liquid phase of CA-4 is 3778 Pa·s and the liquid contents is 86%, which shows significant influence on formation of melt in ash fusion stage.

In order to better account for the fusibility difference between CA and SA, four ash samples were compared in same ternary phase diagram, in which different fields surrounded by black lines represent different primary mineral phases disappearing lastly at T_{liq} (the temperature at which the last solid phase disappears). In Fig. 8, fusibility of CA-1 is same with that of SA-1 located in anorthite (melting point:

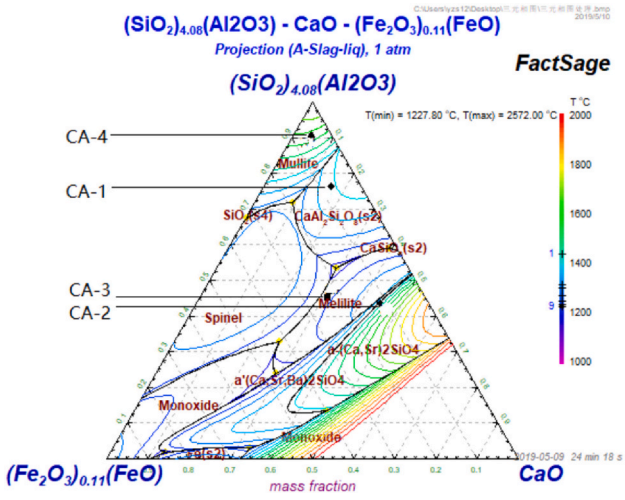


Fig. 8. Ternary phase diagram of $(SiO_2)_{4.08}(Al_2O_3)$-CaO-$(Fe_2O_3)_{0.11}$(FeO).

1553 °C) primary field, which is reasonable to use synthetic ash to simulate the fusibility of coal ash. And there are small differences of the fusibility between CA-2, CA-3 and their synthetic ash, of which chemical compositions located in melilite (melting point: about 1600 °C) primary field. Fusibility of CA-4 is different from that of SA-4, of which chemical composition located in mullite (melting point: 1810 °C) primary field. The liquid content is low for high melting point mineral at certain temperature, which is disadvantageous for mass transfer related to mineral reaction, resulting in different fusibility of coal ash and synthetic ash. Therefore, it can be concluded that a high mineral melting point in the corresponding field in the ternary phase diagram correlates with greater fusibility difference between coal ash and synthetic ash.

4. Conclusion

In this study, four ash samples were selected to compare of fusibility between coal ash and synthetic ash. The main conclusions are summarized as follow:

(1) AFTs of ash with high-calcium-low-iron is similar (< 10 °C) with that of the synthetic one. In case of high-calcium-high (medium)-iron ash, the AFTs of CA-2 and CA-3 are slightly higher (< 75 °C) than that of their synthetic ashes. However, DT, ST and HT of the ash with low-calcium-low-iron are higher (< 75 °C) than that of the synthetic one, while the FT of coal ash is 99 °C lower than that of the synthetic one.
(2) For the ash with high-calcium-low-iron, feldspar is the main mineral in both the coal ash and synthetic one. Formation of gehlenite and akermanite leads to the different fusibility of the ashes with high-calcium-high(medium)-iron. Difference of fusibility of the ash with low-calcium-low-iron is due to formation of mullite, and quartz and corundum.
(3) When liquid viscosity is high or liquid content is low, mineral mass transfer rates of different forms of mineral are different, enlarging different fusibility between coal ash and synthetic ash. The synthetic ash is not suitable to simulate coal ash with low-calcium-low-iron for studying fusibility. The ashes with chemical compositions located in high-melting-temperature region showed an obvious different fusibility between CA and SA.

CRediT authorship contribution statement

Zong-shuai Yuan: Methodology, Data curation, Writing-original draft preparation; **Ji Wang:** Conceptualization, Software, Writing-Reviewing and Editing; **Lingxue Kong:** Visualization, Investigation, Writing-Reviewing and Editing; **Jin Bai:** Supervision, Validation, Writing-Reviewing and Editing; **Zhonghai Ni**, **Huaizhu Li**, **Zongqing Bai**: Supervision; **Wen Li:** Supervision, Validation.

Declaration of competing interest

The authors declare that they have no known competing financial interests or personal relationships that could have appeared to influence the work reported in this paper.

Acknowledgments

This work was financial supported by NSFC-DFG [grant number 21761132032], Joint Foundation of Natural Science Foundation of China and Xinjiang [grant number U1703252], Shanxi Province Science Foundation for Youths [grant number 201901D211589], International Partnership Program of Chinese Academy of Sciences [grant number 122214KYSB20170020].

References

[1] C. Higman, S. Tam, Advances in coal gasification, hydrogenation, and gas treating for the production of chemicals and fuels, Chem. Rev. 114 (2014) 1673–1708.
[2] J. Xu, Y. Yang, Y. Li, Recent development in converting coal to clean fuels in China, Fuel 152 (2015) 122–130.
[3] L. Kong, J. Bai, Z. Bai, Z. Guo, W. Li, Improvement of ash flow properties of low-rank coal for entrained flow gasifier, Fuel 120 (2014) 122–129.
[4] L. Ma, C. Yue, L. Ye, H. Huo, L. Han, L. Chang, W. Bao, J. Wang, Effects of supports on Pd-Fe bimetallic sorbents for Hg-0 removal activity and regeneration performance from coal-derived fuel gas, Energy Fuel 33 (2019) 8976–8984.
[5] W. Li, J. Bai, Chemistry of Ash From Coal, Science Press, Beijing, 2013.
[6] Y. Gong, G. Yu, Q. Guo, Z. Zhou, F. Wang, Y. Liu, Experimental study of the particle deposition characteristics in an entrained flow gasifier, Chem. Eng. Sci. 138 (2015) 291–302.
[7] S.A. Benson, E.A. Sondreal, J.P. Hurley, Status of coal ash behavior research, Fuel Process. Technol. 44 (1995) 1–12.
[8] Z. Xue, Q. Guo, Y. Gong, X. Wu, F. Wang, G. Yu, Detailed deposition characteristics around burner plane in an impinging entrained-flow coal gasifier, Chem. Eng. Sci. 198 (2019) 85–97.
[9] Y. Wang, Y. Xiang, D. Wang, C. Dong, Y. Yang, X. Xiao, Q. Lu, Y. Zhao, Effect of sodium oxides in ash composition on ash fusibility, Energy Fuel 30 (2016) 1437–1444.
[10] Solid Mineral Fuels-Determination of Fusibility of as-High-temperature Tube Method, MOD, Chinese-standard, ISO 540, (1995).
[11] M. Li, F. Li, Q. Liu, Y. Fang, H. Xiao, Regulation of ash fusibility for high ash-fusion-temperature (AFT) coal by industrial sludge addition, Fuel 244 (2019) 91–103.
[12] T. Yan, J. Bai, L. Kong, Z. Bai, W. Li, J. Xu, Effect of SiO_2/Al_2O_3 on fusion behavior of coal ash at high temperature, Fuel 193 (2017) 275–283.
[13] F.E. Huggins, D.A. Kosmack, G.P. Huffman, Correlation Between Ash-fusion Temperatures and Ternary Equilibrium Phase Diagrams, 60 Elsevier, 1981, pp. 577–584.
[14] C. He, J. Bai, A.Y. Ilyushechkin, H. Zhao, L. Kong, H. Li, Z. Bai, Z. Guo, W. Li, Effect of chemical composition on the fusion behavior of synthetic high-iron coal ash, Fuel 253 (2019) 1465–1472.
[15] X. Lin, J. Liu, K. Ideta, J. Miyawaki, Y. Wang, I. Mochida, S. Yoon, Cation induced microstructure and viscosity variation of molten synthetic slag analyzed by solid-state NMR, Fuel 267 (2020) 10.
[16] S.V. Vassilev, C.G. Vassileva, Contents and associations of rare earth elements and yttrium in biomass ashes, Fuel 262 (2020).
[17] S.V. Vassilev, K. Kitano, S. Takeda, T. Tsurue, Influence of mineral and chemical composition of coal ashes on their fusibility, Fuel Process. Technol. 45 (1995) 27–51.
[18] X. Chen, L. Kong, J. Bai, Z. Bai, W. Li, Effect of Na_2O on mineral transformation of coal ash under high temperature gasification condition, J. Fuel Chem. Technol. 44 (2016) 263–272.
[19] G. Liu, S.V. Vassilev, L. Gao, L. Zheng, Z. Peng, Mineral and chemical composition and some trace element contents in coals and coal ashes from Huaibei coal field, China, Energy Convers. Manag. 46 (2005) 2001–2009.
[20] M. Aho, E. Ferrer, Importance of coal ash composition in protecting the boiler against chlorine deposition during combustion of chlorine-rich biomass, Fuel 84 (2005) 201–212.
[21] K.S. Vorres, Melting behavior of coal ash materials from coal ash composition, J. Eng. Power-Trans. ASME 22 (1977) 118–123.
[22] V.R. Gray, Prediction of ash fusion temperature from ash composition for some New Zealand coals, Fuel 66 (1987) 1230–1239.
[23] B. Liu, Q. He, Z. Jiang, R. Xu, B. Hu, Relationship between coal ash composition and ash fusion temperatures, Fuel 105 (2013) 293–300.
[24] T. Sasi, M. Mighani, E. Oers, R. Tawani, M. Graebner, Prediction of ash fusion

behavior from coal ash composition for entrained-flow gasification, Fuel Process. Technol. 176 (2018) 64–75.
[25] N. Jing, H. Zhu, Q. Wang, Effect of chemical compositions on ash fusibility characterization of a Jincheng anthracite during combustion and gasification, Chem. Eng. Commun. 204 (2017) 858–863.
[26] J. Wang, L. Kong, J. Bai, H. Li, Z. Bai, X. Li, W. Li, The role of residual char on ash flow behavior, part 1: the effect of graphitization degree of residual char on ash fusibility, Fuel 234 (2018) 1173–1180.
[27] W. Shi, L. Kong, J. Bai, J. Xu, W. Li, Z. Bai, W. Li, Effect of CaO/Fe_2O_3 on fusion behaviors of coal ash at high temperatures, Fuel Process. Technol. 181 (2018) 18–24.
[28] T. Yan, L. Kong, J. Bai, Z. Bai, W. Li, Thermomechanical analysis of coal ash fusion behavior, Chem. Eng. Sci. 147 (2016) 74–82.
[29] C. He, J. Bai, W. Li, L. Kong, J. Xu, S. Guhl, X. Li, Z. Bai, W. Li, Iron transformation behavior in coal ash slag in the entrained flow gasifier and the application for Yanzhou coal, Fuel 237 (2019) 851–859.
[30] W. Song, L. Tang, X. Zhu, Y. Wu, Z. Zhu, S. Koyama, Effect of coal ash composition on ash fusion temperatures, Energy Fuel 24 (2010) 182–189.
[31] A.Y. Ilyushechkin, S.S. Hla, D.G. Roberts, N.N. Kinaev, The effect of solids and phase compositions on viscosity behavior and T_{CV} of slags from Australian bituminous coals, J. Non-Cryst. Solids 357 (2011) 893–902.
[32] F. Li, J. Huang, Y. Fang, Y. Wang, The effects of leaching and floatation on the ash fusion temperatures of three selected lignites, Fuel 90 (2011) 2377–2383.
[33] K. Han, Z Huang, Z Wang, J Zhou, Action mechanism of sodium compounds in Zhundong coal ash on the process of sintering and fusion, J. Fuel Chem. Technol. 43 (2015) 22–26.
[34] X. Yao, H. Zhou, K. Xu, Q. Xu, L. Li, Evaluation of the fusion and agglomeration properties of ashes from combustion of biomass, coal and their mixtures and the effects of K_2CO_3 additives, Fuel 255 (2019) 11.
[35] B. Zhou, H. Zhou, J. Wang, K. Cen, Effect of temperature on the sintering behavior of Zhundong coal ash in oxy-fuel combustion atmosphere, Fuel 150 (2015) 526–537.
[36] E. Jak, S. Degterov, P.C. Hayes, A.D. Pelton, Thermodynamic modelling of the system Al2O3-SiO2-CaO-FeO-Fe2O3 to predict the flux requirements for coal ash slags, Fuel 77 (1998) 77–84.
[37] C.W. Bale, E. Belisle, P. Chartrand, S.A. Decterov, G. Eriksson, K. Hack, I.H. Jung, Y.B. Kang, J. Melancon, A.D. Pelton, C. Robelin, S. Petersen, FactSage thermochemical software and databases - recent developments, Calphad-Comput. Coupling Phase Diagr. Thermochemistry 33 (2009) 295–311.
[38] X. Chen, L. Kong, J. Bai, Z. Bai, W. Li, Study on fusibility of coal ash rich in sodium and sulfur by synthetic ash under different atmospheres, Fuel 202 (2017) 175–183.
[39] M. Reinmoeller, M. Klinger, E. Thieme, B. Meyer, Analysis and prediction of slag-induced corrosion of chromium oxide-free refractory materials during fusion of coal and biomass ash under simulated gasification conditions, Fuel Process. Technol. 149 (2016) 218–230.